1
Immunological Evolution of Catalysis

Jun Yin, Peter G. Schultz

1.1
Introduction

Both antibodies and enzymes are able to bind a large number of ligands, ranging from small molecules to macromolecules, with high affinity and specificity. Pauling was the first to note that the fundamental difference between the two is that enzymes evolve to selectively bind high-energy transition states and are selected based on catalytic efficiency, whereas antibodies evolve to maximize the affinity for molecules in their ground state [1, 2]. A logical consequence of this comparison is that an antibody generated to a stable analog of a rate-limiting transition state for a particular reaction should act as a selective enzyme-like catalyst. Indeed, there are now many examples in which, with the appropriate chemical instruction, antibodies have been generated that catalyze a large number of reactions, ranging from pericyclic reactions to carbonium ion rearrangements [3]. Importantly, detailed structural and functional studies of the immunological evolution of catalytic antibodies have provided important insights into the evolution of binding energy and catalysis in biological systems. Here we focus on a number of such studies that have been carried out in this laboratory.

1.2
Parallels between Antibody and Enzyme Evolution

There are many parallels between the immunological evolution of antibodies and the natural evolution of enzymes (Table 1.1). Both processes involve genetic recombination and point mutation coupled with a selection process during which molecules with desired function are identified from a large diverse library of proteins. In the case of enzymes, gene duplication and exon shuffling provide proteins with new structures and functions [4, 5]. Random mutations further increase molecular diversity and refine biological function. Similar mechanisms are responsible for the diversity of the antibody molecule (Fig. 1.1) [6–8]. Antibody genes are segmented and exist as groups with multiple members. For an example, in the murine genome there are four functional joining (J) segments for the light chain variable region and four for

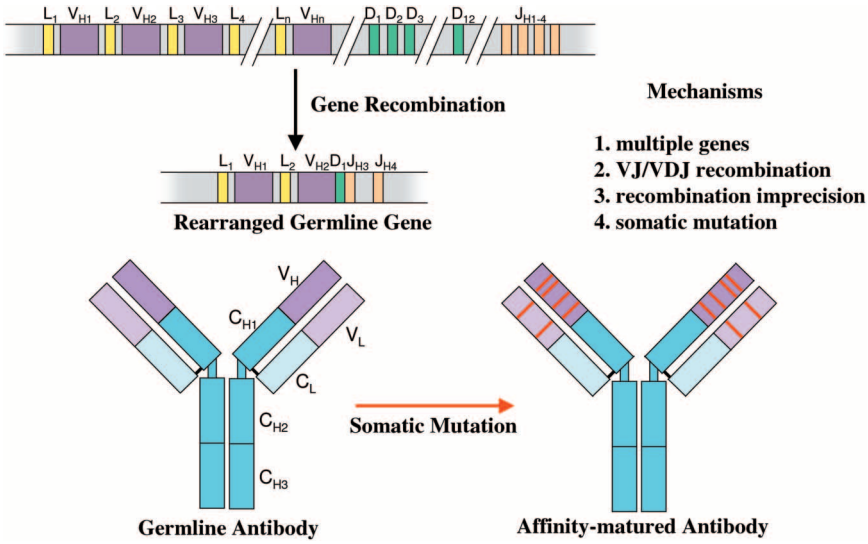

Fig. 1.1 The generation of immunological diversity by genetic recombination and somatic mutation.

the heavy chain, at least 12 diversity (D) segments, hundreds of light chain variable (V_L) segments and heavy chain variable (V_H) segments. Genes for the antibody light and heavy chain variable regions are assembled by the random recombination of V, (D) and J segments; random association of light and heavy chain genes give rise to the germline antibody repertoire. Moreover, the exact site of the joining between segments during gene recombination is imprecise and leads to junctional diversity at the V-(D)-J junctions. Nucleotides can be deleted from or added randomly to both ends of the D gene segments, leading to CDR H3 length variations and even greater variability at the joining region. After the combinatorial assembly of the antibody genes, the germline antibody undergoes affinity maturation during which somatic mutations are introduced throughout the antibody variable domain, further expanding the sequence diversity of the germline antibody repertoire. As a result, the immune system has the potential to generate more than 10^{11} unique antibodies [9] that possess high affinity and specificity toward virtually any ligand.

Despite the similarities in the mechanism used to generate molecular diversity, the two evolutionary processes operate on very different time scales: enzymes typically evolve over millions of years; in contrast, antibody binding energy evolves over a period of weeks. The immunological evolution of a catalytic antibody in which immunological evolution is programmed with chemical information about the rate-limiting transition state of a reaction bridges the gap between these two processes. Indeed, antibodies have been generated that recapitulate the catalytic efficiencies, selectivities, and even mechanisms of enzymes in a number of instances [10, 11]. In other cases, catalytic antibodies have been generated for reactions that are not known to exist in Nature [12, 13].

Because the immune response occurs over a time scale of weeks, one has the opportunity to characterize the entire evolutionary process – from the germline precursor to the affinity-matured catalytic antibody. Such an analysis would allow us to address some fundamental questions regarding the evolution of binding energy and catalysis both in immune response and in the evolution of enzymes. For example, (1) How does the immunoglobulin fold bind so many different chemical structures with high affinity and specificity? Is the binding potential of the antibody molecule a result of sequence diversity alone or are some other mechanisms also operating? Similarly, since more than a hundred reactions have been shown to be catalyzed by antibodies, how does the antibody combining site manage to accommodate such a wide array of catalytic mechanisms? (2) Are there any differences between the binding mode of the germline and that of the affinity-matured antibodies to antigens and what are the functional roles of the somatic mutations, both in the antibody combining site and distal to it, that lead to high affinity and high specificity binding in the affinity-matured antibodies? (3) How do binding energy and catalysis coevolve during the process of immunological evolution of catalytic antibodies, and does this process provide insights into the mechanisms of enzyme evolution?

1.3
Evolution of Catalytic Antibodies

In order to characterize the immunological evolution of catalytic antibodies, both the germline and the affinity-matured antibodies are cloned, sequenced and expressed as the Fab (Fragment, antigen binding) [14]. The sites and identities of the somatic mutations are determined by sequence alignments, and their functional roles can be analyzed by site-directed mutagenesis of the germline and affinity-matured Fab. High resolution X-ray crystal structures of the germline Fab and the affinity-matured Fab with and without hapten bound provide an opportunity to analyze the underlying structural basis for the evolution of binding energy and catalysis. To date, such detailed studies of the immunological evolution of catalytic antibodies have been carried out with five catalytic antibody systems: esterase antibody 48G7 [15–18], Diels-Alderase antibody 39A11 [19–21]oxy-Cope antibody AZ28 [12, 22, 23], sulfur oxidase antibody 28B4 [24–26], and ferrochelatase antibody 7G12 [27–30]. These antibodies were raised against haptens of distinct structures and catalyze a variety of reactions.

1.4
Ferrochelatase Antibody 7G12 – Evolution of the Strain Mechanism

The enzyme ferrochelatase catalyzes the insertion of Fe^{2+} into protoporphyrin IX as the last step in heme biosynthetic pathway [31]. *N*-alkylporphyrins, in which the porphyrin macrocycle is distorted because of alkylation at one of the pyrrole nitrogen atoms, are strong inhibitors of this enzyme [32]. Based on this observation, it was thus proposed that the enzyme catalyzes the porphyrin metalation reaction by distorting

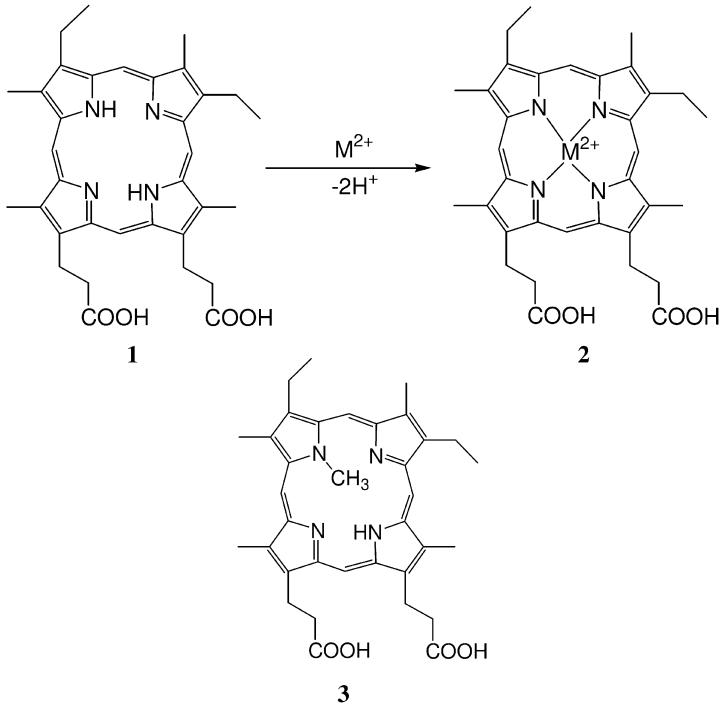

Scheme 1.1

the porphyrin substrate out of planarity so that the pyrrole nitrogen lone pairs are more accessible for metal chelation [33]. To test this notion, antibody 7G12 was generated against an analog of the strained substrate, *N*-methylmesoporphyrin (**3**) (NMP), and was found to catalyze the metalation of mesoporphyrin (**1**) (MP) by Zn^{2+} with rates comparable to that of the natural enzyme (Scheme 1.1) [27]. The same antibody also catalyzes the insertion of Cu^{2+} into mesoporphyrin at a lower rate. Resonance Raman spectroscopy shows that antibody 7G12 induces distortion in the bound mesoporphyrin substrate corresponding to an alternative up-and-down tilting of the two opposite pyrrole rings [34]. In contrast, the enzyme ferrochelatase induces tilting of all four pyrrole rings in the same direction (doming) [34].

In order to determine the precise conformation of the porphyrin substrate in the antibody combining site, we solved the X-ray crystal structure of 7G12 Fab-MP Michaelis complex to 2.6 Å resolution [29]. Crystals of 7G12 Fab-MP complex give intense red fluorescence upon irradiation with green excitation light around 546 nm (Fig. 1.2). The addition of copper acetate to the crystallization drop leads to a rapid loss of fluorescence due to the formation of the non-fluorescent Cu(II)MP complex, demonstrating that the antibody-MP cocrystal is catalytically active. The F_o–F_c electron density map clearly shows that the substrate MP molecule adopts a non-planar conformation (Fig. 1.3); the out-of-plane displacements for the substrate MP and the hapten NMP are shown in Fig. 1.4. All pyrroles in MP show significant displacements away from the porphyrin least-squares (PLS) plane. Pyrrole A in MP adopts a similar angle (26°)

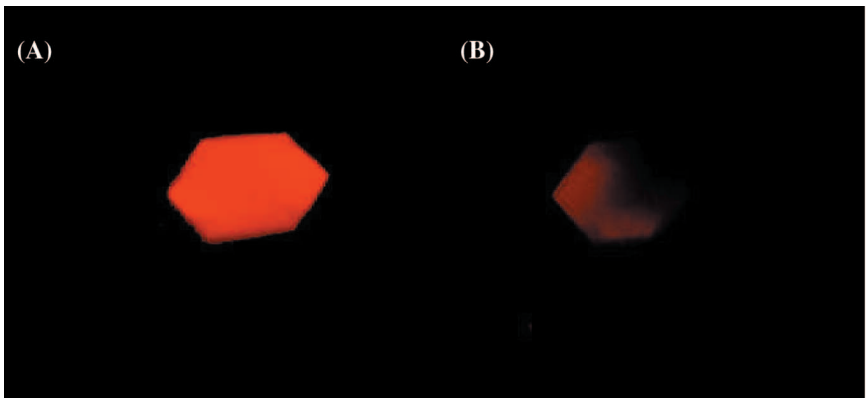

Fig. 1.2 Fluorescent micrographs of a single crystal of 7G12 Fab-MP complex (**A**) before and (**B**) after the addition of copper acetate.

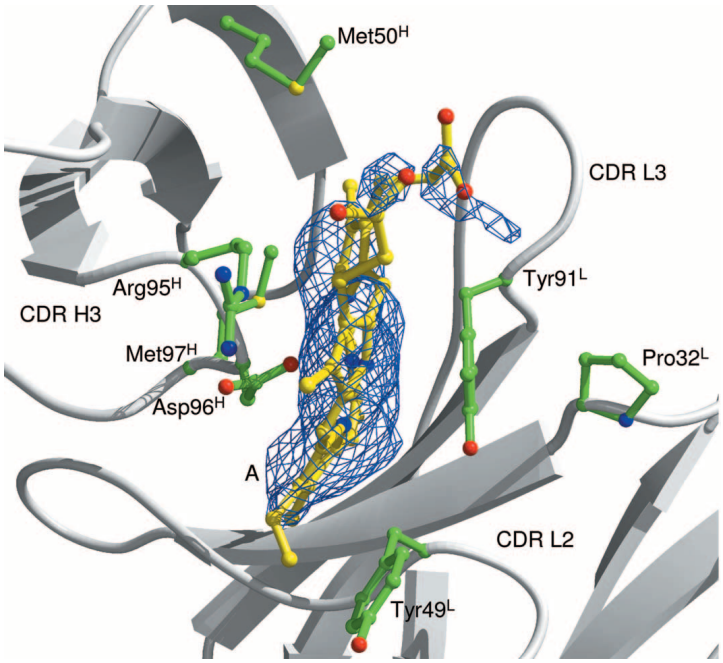

Fig. 1.3 F_o–F_c electron density map contoured at 2.00 for the substrate MP molecule (colored in yellow) bound with 7G12 Fab. Residues making important packing interactions with MP in the antibody combining site are also shown.

relative to the PLS plane to that observed in NMP [28], however, the other pyrrole rings form larger angles to the PLS plane than do their NMP counterparts (16°, 17°, and 25° for rings B, C, and D, respectively). The porphyrin conformation observed in the crystal structure of Fab-MP complex agrees with prior resonance Raman spectroscopy

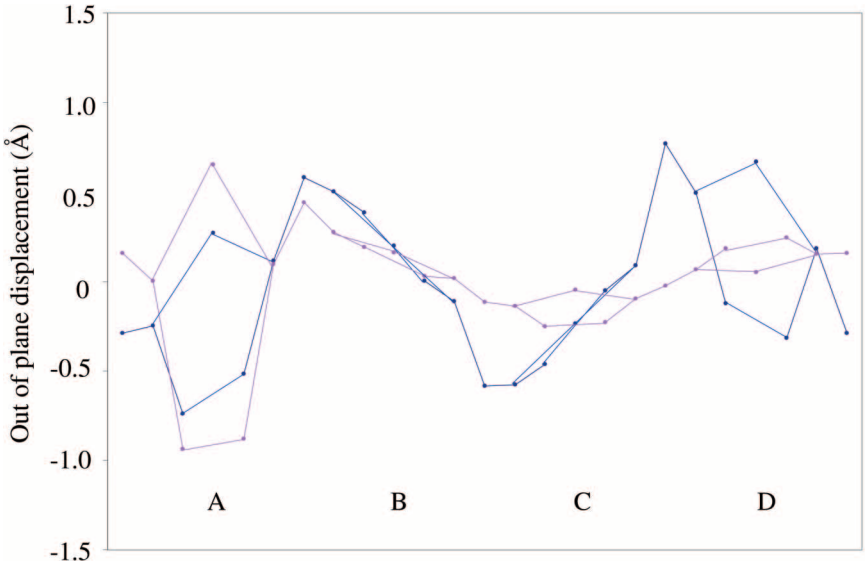

Fig. 1.4 Out-of-plane displacement of porphyrin ring atoms from the porphyrin least-squares (PLS) plane for MP (blue) and NMP (pink) bound to antibody 7G12. The porphyrin atoms that are involved in the same pyrrole ring are connected to give a pentagon shape. **A**, **B**, **C**, and **D** denote the porphyrin pyrroles.

data, which indicates an up-and-down tilting of the pyrrole rings, based on the observation of specific out-of-plane vibration mode [34]. A normal mode decomposition (NCD) analysis, which deconstructs porphyrin deformations into low-frequency normal coordinate displacements [35], shows a moderate doming (A2u) deformation, as well as strong saddling (B2u) and ruffling (B1u) deformations for the antibody-bound MP.

An analysis of the crystal structure of the 7G12 Fab-substrate MP complex reveals those interactions between the residues in the antibody combining site and MP that lead to substrate distortion (Fig. 1.3). The porphyrin molecule is bound in a cleft, with CDR L2 and CDR L3 forming one side of the cleft and CDR H3 forming the other side. Part of the CDR H3 loop, composed of $Arg95^{H}$, $Asp96^{H}$ and $Met97^{H}$, packs on the macrocyclic ring of the porphyrin. The carboxylic oxygen of $Asp96^{H}$ points toward the center of the porphyrin ring and is within hydrogen-bonding distance of all pyrrole nitrogen atoms. The guanidino group of $Arg95^{H}$ forms salt bridges with both carboxylates of the propionic acid side chains of the porphyrin ring. The aromatic side chains of $Tyr49^{L}$ and $Tyr91^{L}$π stack on pyrrole rings A and B of the substrate. While the π stacking interaction on one face of pyrrole ring B is balanced by the packing of $Asp96^{H}$ on the other face, the π stacking interaction with $Tyr49^{L}$ pushes pyrrole ring A out of plane because of the absence of heavy chain residue contacts on the opposite face. In the crystal structure of Fab-hapten NMP complex, $Tyr49^{L}$ also packs against *N*-methyl pyrrole, which is distorted out of plane of the other pyrrole rings because of the *N*-methyl substitution [28]. Thus, the distortion

of the MP substrate induced by the antibody combining site is a direct result of the distortion in NMP induced by *N*-methyl substitution on the free MP. The active site of antibody 7G12 reflects the "instruction" from the hapten NMP during the process of immune response *in vivo* and acts to strain the MP substrates *in vitro* and catalyze porphyrin metalation.

Modern theories of biological catalysis date from Haldane's 1930 treatise "Enzymes", in which he first proposed the strain theory: "using Fischer's lock-and-key simile, the key does not fit the lock perfectly but exercises a certain strain on it" [36]. In other words, a degree of misfit between the enzyme and its bound substrate is needed to distort the substrate toward the transition state conformation. Although the notion that enzymes use binding energy to strain or distort substrates is a fundamental theory of enzyme catalysis, it has proven difficult to validate experimentally [37]. The crystal structure of the 7G12 Fab-MP Michaelis complex provides unequivocal structural evidence for the strain theory proposed by Haldane more than seventy years ago. Thus, the study on the evolution of catalytic antibody not only yields new biological catalysts, but also tests and validates fundamental principles of enzyme catalysis. In addition, the detailed structural and biophysical characterization of the germline and affinity-matured antibodies should provide a detailed mechanistic picture of the evolution of this strain mechanism.

The germline precursor of antibody 7G12 accumulates five somatic mutations during affinity maturation: two in the V_L chain: $Ser14^L Thr$ and $Ala32^L Pro$; three in V_H: $Arg50^H Met$, $Ser76^H Asn$ and $Ser97^H Met$ [28]. The X-ray crystal structures of the Fab fragment of the germline and affinity-matured antibody both unbound and hapten NMP-bound were solved to high resolution [29]. Superposition of the crystal structures of the unliganded and NMP-bound germline Fab shows that there are significant conformational changes in the loop of CDR H3 upon hapten binding (Fig. 1.5A). In the unliganded germline Fab, CDR H3 adopts a relaxed and extended conformation. The side chains of $Arg95^H$ and $Asp96^H$, which are at the tip of

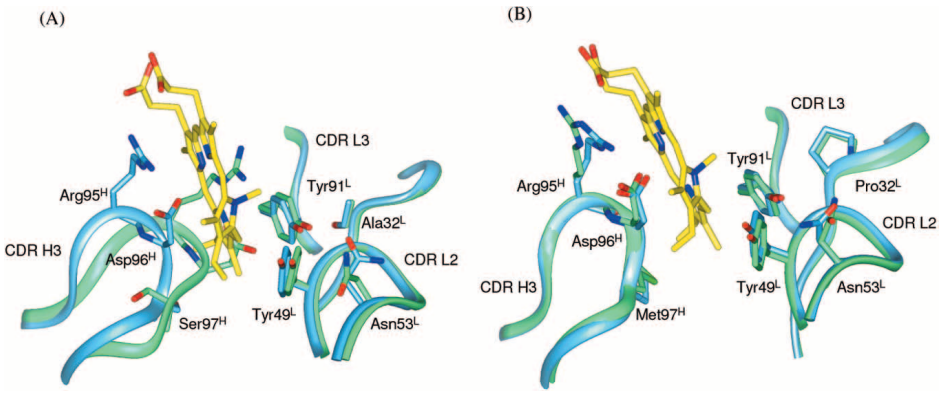

Fig. 1.5 (**A**) Overlay of the unliganded germline Fab (green) of antibody 7G12 and the germline Fab-hapten NMP **3** complex (blue). (**B**) Overlay of the unliganded affinity-matured Fab (green) of antibody 7G12 and the affinity-matured Fab-hapten NMP **3** complex (blue). Hapten **3** is in yellow.

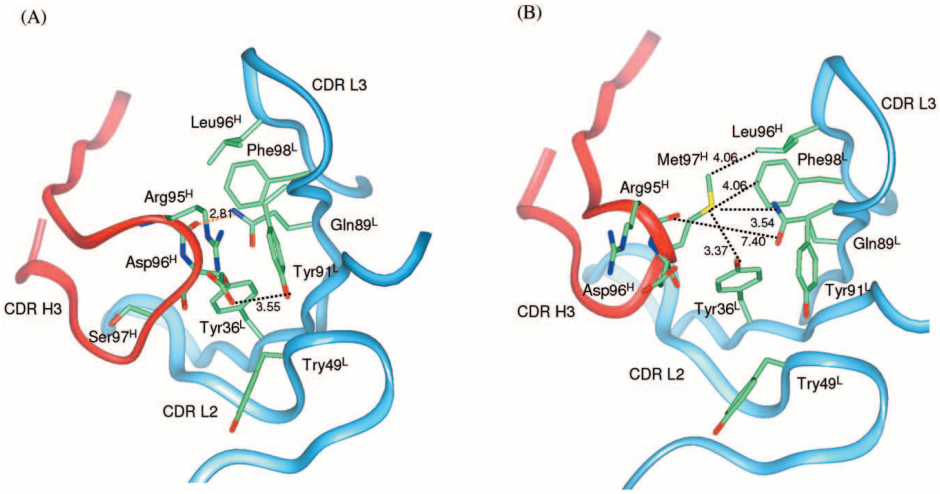

Fig. 1.6 (**A**) In the 7G12 germline Fab without NMP bound, CDR H3 extends into the antibody combining site, and a hydrogen bond (red dotted lines) is formed between the backbone CO of $Arg95^H$ and carboxamide NH of $Gln89^L$. (**B**) In the 7G12 affinity-matured Fab without NMP bound, CDR H3 is kinked because of $Ser97^H$Met somatic mutation, and the antibody combining site is preorganized for NMP binding. Dotted lines with numbers show the distance (Å) between the two atoms. NMP is in yellow.

CDR H3 loop, move into the hapten-binding site, occupying the space taken by the hapten in the germline Fab-NMP complex. There is a hydrogen bond between the backbone carbonyl oxygen of $Asp96^H$ and carboxamide NH of $Gln89^L$ (Fig. 1.6A). Upon NMP binding, the backbone of CDR H3 loop is pushed backward toward the side of the heavy chain by roughly 4 Å (at Cα of $Arg95^H$) because of the insertion of NMP molecule into the hapten-binding pocket. There is even larger movement for the side chains of $Arg95^H$ (7.0 Å at the guanidino C) and $Asp96^H$ (5.5 Å at the carboxamide C) upon NMP binding. In the germline Fab-NMP complex, $Arg95^H$ packs onto the macrocyclic ring of NMP and the carboxylate group of $Asp96^H$ is positioned equidistant from the four pyrrole nitrogen atoms of NMP (2.6–3.0 Å) and may form hydrogen bonds with one or more of the pyrrole NH groups. The structural flexibility of germline antibody is also manifested by comparing the electrostatic surface of the antibody combining site before and after the binding of NMP (Fig. 1.7). In the hapten-free form, the germline antibody combining site is flat with minor electrostatic charges distributed on the surface. However, upon hapten binding, the movement of the CDR H3 loop creates a cavity on the surface of the germline antibody that complements the shape of the distorted porphyrin molecule. Exposure of residues $Arg95^H$ and $Asp96^H$ also introduces negative charges inside the cavity and positive charges at the rim, which complement the charge distribution of NMP. These results suggest the germline antibody of 7G12 adopts an "induced fit" binding mode and the conformational changes in the germline antibody upon hapten binding lead to enhanced complementarity between the antibody combining site and the hapten.

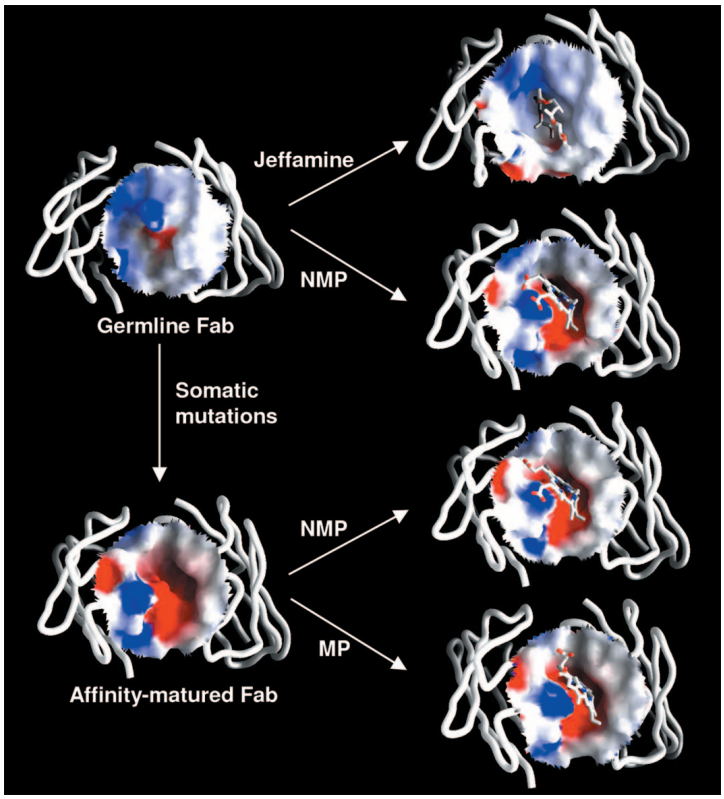

Fig. 1.7 Electrostatic surface potential of the antibody combining site in the germline and affinity-matured Fab either unliganded or bound with NMP, MP or jeffamine. The red and blue correspond to negative and positive surface potential, respectively.

The conformational flexibility of the germline antibody is further confirmed by a crystal structure of the germline Fab-jeffamine complex [30].

Jeffamine ($CH_3OCH_2CH_2O(CH(CH_3)CH_2O)_nCH_2CH(NH_2)CH_3$, $n \approx 8$), which is structurally very distinct from the hapten NMP, was found to bind the germline antibody of 7G12 but not the affinity-matured antibody. The crystal structure of the germline Fab-jeffamine complex shows that five isopropoxy units of the jeffamine molecule fold into a U-shaped conformation and are deeply embedded in the antibody combining site consisting of mainly hydrophobic residues including $Tyr36^L$, $Leu46^L$, $Tyr49^L$, $Tyr91^L$, $Leu96^L$ and $Phe98^L$ from the light chain and $Thr93^H$ and $Trp100^H$ from the heavy chain (Fig. 1.8). A hydrogen bond is formed between O6 of jeffamine and the indole Nε1 of $Trp100^H$ (2.8 Å). $His35^H$ and $Arg95^H$ also pack on the poly(isopropoxy) backbone of the jeffamine molecule. Superposition of the unliganded germline Fab and the germline Fab with bound jeffamine or bound hapten NMP reveals that the heavy chain CDR loops undergo an even larger rearrangement upon binding jeffamine than the binding of NMP (Fig. 1.9A). The Cα of $Asp96^H$ of CDRH3 moves 10.9 Å away from the light chain in order to accommodate jeffamine.

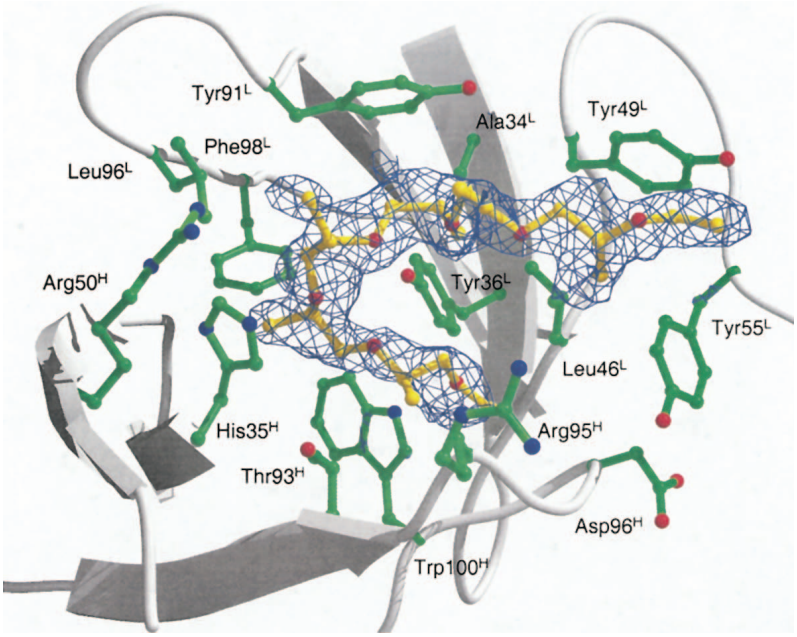

Fig. 1.8 F_o–F_c electron density map contoured at 2.00 for the jeffamine molecule (colored in yellow) bound to the germline Fab of antibody 7G12. Residues making important packing interactions with jeffamine in the antibody combining site are also shown.

This forces a conformational change of CDRH1 to avoid steric clashes between the phenol residue of $Tyr27^H$ and the carboxyl group of $Asp96^H$. As a result of antibody combining site reorganization, two different sets of residues are used by the germline antibody to interact with either NMP or jeffamine (Fig. 1.10). The charge distribution and the shape of the antibody combining site in the germline Fab-jeffamine complex is very different from the that of the same antibody when there is no ligand bound or with its hapten NMP bound (Fig. 1.7). Thus the germline antibody of 7G12 has an intrinsic conformational flexibility in the heavy chain CDR loops; binding of either hapten or structurally distinct ligands induces CDR loop rearrangements that increase complementarity between the antibody and the ligands. Importantly, the conformational diversity of the germline antibody gives rise to binding polyspecificity and plays a significant role in expanding the germline-binding repertoire.

In contrast to the germline antibody, a comparison of the crystal structures of the unliganded and NMP-bound 7G12 Fab indicates that minimal changes occur upon hapten binding in the affinity-matured antibody (Fig. 1.5B). Neither the shape nor the electrostatic characteristics of the antibody combining site of the affinity-matured antibody change significantly upon the binding of the hapten or the substrate molecule (Fig. 1.7), suggesting that the antibody combining site in the affinity-matured Fab is rigid and preorganized for the binding of distorted porphyrins. This "lock-and-key" binding mode [38] of the affinity-matured antibody versus "induced fit" binding [39]

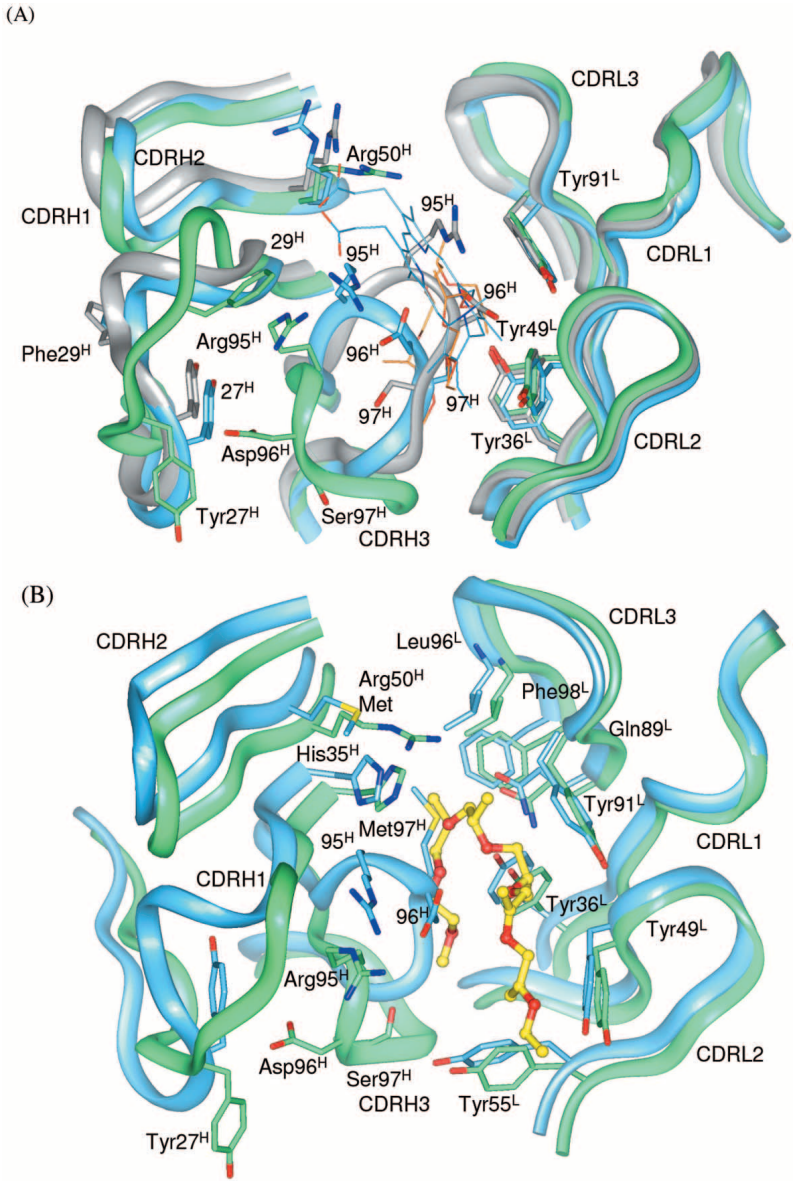

Fig. 1.9 (**A**) Overlay of the unbound germline Fab (gray) of antibody 7G12, the germline Fab-NMP complex (blue), and the germline Fab-jeffamine complex (green). The heavy chain CDR loops of the germline antibody undergoes significant conformational changes upon the binding of NMP (blue lines) or jeffamine (orange). (**B**) Overlay of the germline Fab-jeffamine complex (green) and the unliganded affinity-matured Fab (blue). Jeffamine is drawn in yellow and in ball and stick.

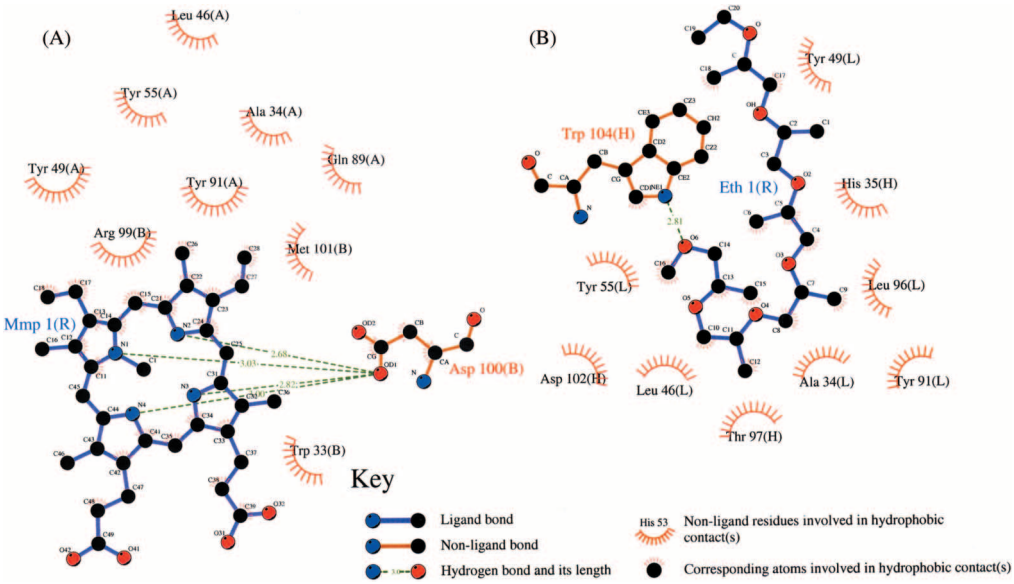

Fig. 1.10 Active-site residues responsible for the binding with **(A)** NMP and **(B)** jeffamine in the antibody combining site of the 7G12 germline Fab.

in the germline antibody was previously observed in the antibodies 48G [17], AZ28 [23] and 28B4 [26]. In all cases, the affinity-matured antibodies show between 40 (AZ28) and more than 30 000 (48G7) times higher hapten-binding affinity relative to the germline antibody. The decrease in K_d and the correspondingly more negative free energy of binding (ΔG) partially originate from a more favorable entropy term ($-T\Delta S$) due to a preorganized combining site. The conformational flexibility of the germline antibody leads to a higher entropic penalty for binding of ligand, since side-chain motion must be restricted upon complex formation.

The structural rigidity in the affinity-matured antibody of 7G12 is also manifested in catalysis [29]. When the substrate MP binds to the affinity-matured antibody 7G12, it is forced to adopt a strained conformation in order to fit the antibody combining site (Fig. 1.7), rather than the antibody combining site reorganizing to accommodate the substrate in its planar conformation. Analysis of the crystal structures of the germline and affinity-matured Fab also provides insights into the mechanism by which this strain mechanism evolved. The somatic mutation $Ser97^{H}Met$ is located in CDR H3 and leads to a sharp turn in the backbone of CDR H3 in the affinity-matured Fab resulting from the packing interactions of $Met97^{H}$ with the side chains of $Tyr36^{L}$, $Gln89^{L}$, $Leu96^{L}$ and $Phe98^{L}$ (Fig. 1.6B). This maintains the position of CDR H3 loop out of the active site and places residues $Arg95^{H}$ and $Asp96^{H}$ in the proper positions to interact with the NMP molecule upon its binding to the affinity-matured antibody. Thus, somatic mutation $Ser97^{H}Met$ fixes the conformation of CDR H3 for NMP binding; in its absence in the germline antibody the CDR H3 loop is flexible.

The same somatic mutation also renders the affinity-matured antibody with higher binding specificity: the side chain of Met97^{H} occupies the position that C10 to C14 of jeffamine binds in the germline antibody and at the same time fixes the conformation of CDR H3 for specific NMP recognition (Fig. 1.9B). As a result, the affinity-matured antibody does not bind jeffamine to any measurable degree, but has almost 100-fold higher affinity for NMP than the germline antibody. The methionine side chain introduced by the Arg50^{H}Met somatic mutation packs against the imidazole ring of His35^{H} and orients its side chain to pack against Met97^{H}, which plays an important role in organizing the conformation of CDR H3 for hapten binding. Thus, somatic mutation Arg50^{H}Met in combination with the Ser97^{H}Met somatic mutation helps to fix the conformation of CDR H3. Finally, the Ala32^{L}Pro somatic mutation increases the steric bulk of the residue at this site in order to reinforce the packing interactions of the antibody with the hapten (Fig. 1.5). In the affinity-matured Fab, Pro32^{L} packs on Tyr49^{L}, which packs directly on pyrrole ring A of NMP bound to the antibody and plays a crucial role in forcing pyrrole A out of the plane of the porphyrin ring in the Fab-MP complex (Fig. 1.3).

The hapten binding and catalytic properties of the germline Fab, affinity-matured Fab and a number of somatic mutants were measured to determine how the structural changes associated with affinity maturation affect binding and catalysis [29]. The 7G12 Fab binds NMP with a dissociation constant (K_d) of 20.7 nM, 95-fold lower than the K_d of the germline Fab (1.96 μM). The value of k_{cat}/K_m of the antibody-catalyzed porphyrin metalation reaction also increases 92-fold from the germline Fab to the affinity-matured Fab. Somatic mutation Ser97^{H}Met fixes the conformation of CDR H3 and preorganizes the antibody combining site for the binding of a strained porphyrin molecule. The Met97^{H}Ser mutant of the affinity-matured Fab reverses this somatic mutation and results in a more flexible antibody combining site that should exert less strain on a porphyrin substrate. Consistent with the structural analysis, the Met97^{H}Ser mutant has a K_d of 373 nM for the binding of NMP, an 18-fold decrease in binding compared to the affinity-matured Fab. Also, this mutant catalyzes the insertion of Cu^{2+} into MP with a K_m of 191 μM and a k_{cat} of 2.2 h^{-1}, corresponding to a virtually unchanged K_m and a tenfold reduced k_{cat} relative to the affinity-matured Fab (K_m = 150 μM and k_{cat} = 24.2 h^{-1}). This suggests that the structural flexibility introduced into the antibody combining site by Met97^{H}Ser mutation does not affect the binding of the Fab to the substrate in the planar ground state (K_m unchanged), but decreases the ability of the antibody combining site to distort the substrate toward the non-planar transition state. This is manifested by an additional 1.4 kcal/mol free energy of activation for the Met97^{H}Ser-catalyzed reaction compared to the affinity-matured antibody. Thus, the catalytic activity for porphyrin metalation appears to have evolved as a consequence of binding affinity for a distorted porphyrin (NMP). Somatic mutations lead to a rigid antibody combining site preorganized to bind the substrate MP in a strained, nonplanar conformation. However, the ability to bind porphyrin in a distorted conformation is compromised in the germline Fab because of the structural flexibility in the antibody combining site, resulting in a correspondingly lower catalytic activity. In summary, the affinity maturation of antibody 7G12 in response to the strained substrate mimetic NMP resembles the evolution of

enzymatic function, in which binding energy is evolved to lower the activation energy of a reaction, in this case by straining the substrate.

Similar examples of conformational plasticity can be found in other proteins, allowing them to bind a large number of different protein and small molecule ligands using the same molecular surface. For an example, human growth hormone (hGH) not only binds and activates human growth hormone receptor (hGHR) but also binds and activates prolactin receptor despite the low sequence identity between hGH and prolactin (23%) as well as between their receptors (28%) [40]. Structural analysis of hGH-hGHR complex and hGH-prolactin receptor complex shows that hGH uses virtually the same set of contact residues to bind both partners. Recently it was shown that the hinge region on the Fc fragment of human immunoglobulin G interacts with four different protein scaffolds that bind at a common site between the C_{H_2} and C_{H_3} domains [41]. Moreover, some enzymes such as hexokinase [42, 43] and triosephosphate isomerase [44] function by an induced fit mechanism in which binding of substrate induces a conformational change in the active site that leads to enhanced catalytic rate. Perhaps this structural plasticity is a remnant of early proteins. The ability of a receptor to alter conformation to bind multiple ligands would have allowed a limited number of proteins to bind a large number of ligands or substrates. Point mutations, like somatic mutations during the affinity-maturation of antibodies, coupled with the proper selection pressure, would then fix a particular active site conformation to bind a specific ligand or catalyze a particular reaction. Indeed the ability to evolve so many different binding and catalytic activities from the antibody framework reinforces this hypothesis for the evolution of protein function.

Not only do studies of catalytic antibodies provide insights into the evolution of the binding and catalytic function of enzymes, they also provide fundamental insights into the molecular basis of the immune response itself. Over half a century ago there was considerable debate over the mechanisms by which the immune system is able to evolve selective, high affinity receptors for an almost infinite number of ligands. Once it was established that the immune system produces a large number of antibodies with different sequences through recombination and somatic mutation, sequence diversity was widely accepted as the basis for the tremendous binding potential of antibody repertoire. However, Haurowitz, Pauling, and others argued that conformational diversity could also account for the virtually infinite binding potential of the antibody molecule [45, 46]. Just as a human hand can bind and adapt its shape to a large number of structures, so could an antibody active site change its shape to complement a virtually infinite number of ligands. This theory was termed the chemical instruction theory. Our studies on the process of antibody affinity maturation reveals that conformational diversity does indeed play a key role in expanding the structural diversity of the germline antibody repertoire, allowing the germline antibody to adopt many different structures (and ligand binding modes). The somatic mutations acquired by the affinity-matured antibody act to both fix the conformation of the CDR loops for specific hapten binding and to introduce side chains that interfere with the binding of non-hapten ligands so as to render the affinity-matured antibody more specific. This may be a general strategy used by the immune system to achieve both highly diverse germline antibody binding repertoire

while at the same time allowing rapid selection for antibodies with high affinity and specificity.

1.5
Esterase Antibody 48G7 – Effect of Distant Mutations on Catalysis

Antibody 48G7 was raised against *p*-nitrophenyl phosphonate transition state analog (**8**) and catalyzes the hydrolysis of the corresponding *p*-nitrophenyl ester and carbonate (**4**) with rate accelerations exceeding 10^4-fold (Scheme 1.2) [15]. Nine somatic mutations were accumulated during the affinity maturation process of antibody 48G7, six in the heavy chain (Glu42^{H}Lys, Gly55^{H}Val, Asn56^{H}Asp, Gly65^{H}Asp, Asn76^{H}Lys, and Ala78^{H}Thr) and three in the light chain (Ser30^{L}Asn, Ser34^{L}Gly, and Asp55^{L}His) [15]. The affinity-matured Fab of 48G7 binds hapten with a K_d of 4.5 nM, whereas its germline precursor Fab has a K_d of 135 μM, 30 000 times higher than the affinity-matured Fab. For the antibody-catalyzed ester hydrolysis reaction, the affinity-matured Fab has a k_{cat}/K_m value 100-fold higher than the germline Fab [15].

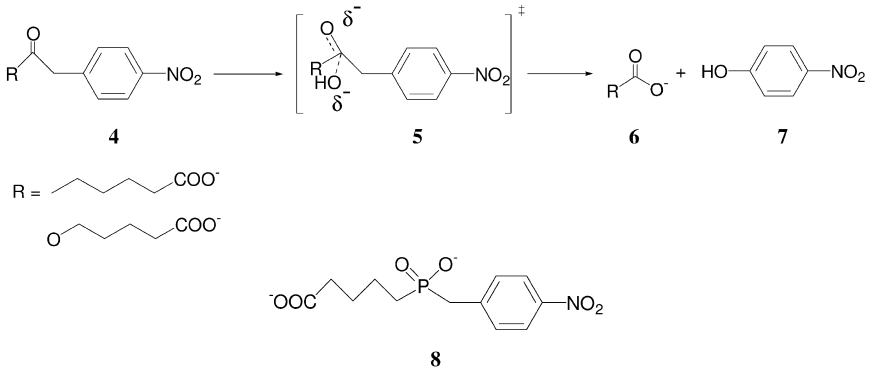

Scheme 1.2

Comparison of the X-ray crystal structures of the unliganded and hapten **8** complexed 48G7 Fab reveals that very few structural changes occur in the affinity-matured antibody upon hapten binding (Fig. 1.11B). In contrast, binding of hapten **8** to the germline Fab again leads to significant conformational changes in the antibody combining site, especially in CDR H3 [17] (Fig. 1.11A): the side chain of Tyr99^H on CDR H3 moves 6 Å away from the hapten binding site at phenyl OH to make room for the incoming hapten, and the side chain of Tyr98^H moves 8.3 Å at phenyl OH and inserts between Tyr99^H and Tyr33^H, which also moves toward the phosphonate group of the hapten. These movements establish a π-cation interaction between the side chains of Arg46^L and Tyr99^H, a π–π interaction between the aryl groups of Tyr99^H and Tyr98^H, and a T-stack interaction between the aryl rings of Tyr98^H and Tyr33^H. All these interactions help to stabilize the conformation of the CDR loops in the germline antibody for hapten binding.

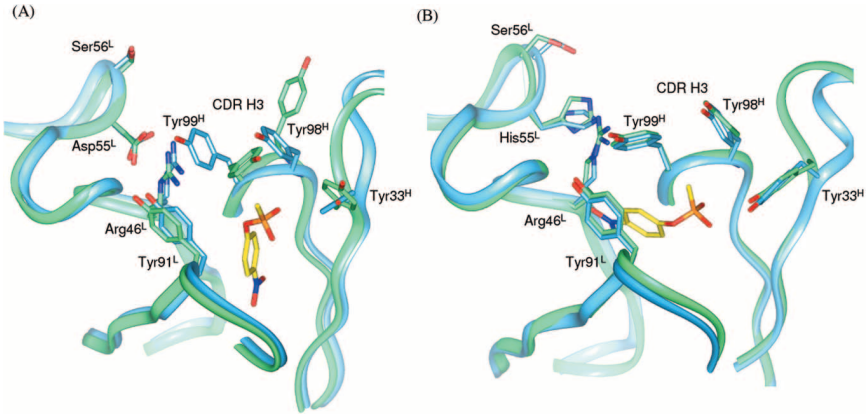

Fig. 1.11 (**A**) Overlay of the unliganded germline Fab (green) of antibody 48G7 and the germline Fab-hapten **8** complex (blue). (**B**) Overlay of the unliganded affinity-matured Fab (green) of antibody 48G7 and the affinity-matured Fab-hapten **8** complex (blue). Hapten **8** is in yellow.

However, in the affinity-matured antibody, the same CDR loop conformations are fixed by somatic mutations, and, as a result, the antibody combining site is preorganized for hapten binding. Two somatic mutations, $Gly55^{H}Val$ and $Asn56^{H}Asp$, are mainly responsible for fixing the conformation of CDR H1, CDR H2 and CDR H3 in the affinity-matured antibody, despite the fact that both of them are some 15 to 20 Å from the bound hapten (Fig. 1.12). Somatic mutation $Gly55^{H}$ Val changes the back-

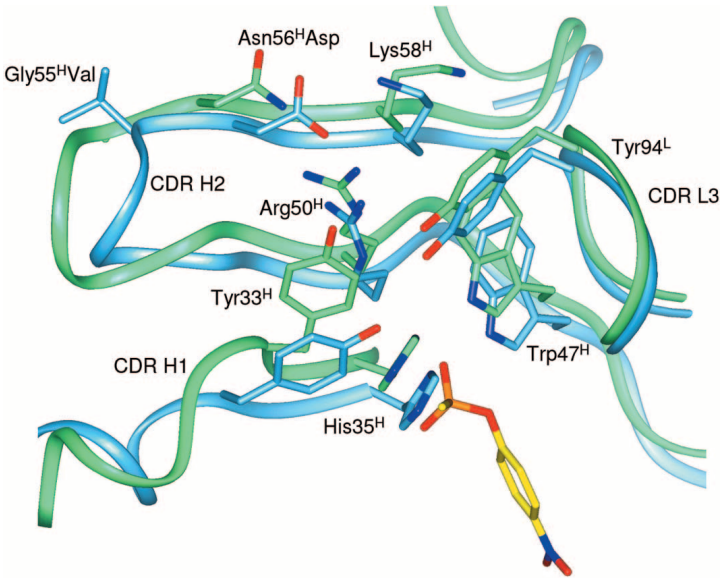

Fig. 1.12 Superposition of the structures of the 48G7 germline Fab-hapten **8** complex (green) and the affinity-matured Fab-hapten **8** complex (blue), illustrating the changes that occur as results of somatic mutations $Gly55^{H}Val$ and $Asn56^{H}Asp$. Hapten **8** is in yellow.

bone conformation of CDR H2 loop and leads to two salt bridges formed between the ε-amino group of Lys58^{H} and the carboxyl group of Asp56^{H} which is introduced by Asn56^{H}Asp somatic mutation. These interactions stabilize the conformation of Asp56^{H} which is part of the hydrogen bond network involving Asp56^{H}, Arg50^{H}, Tyr33^{H}, His35^{H}, Trp47^{H}, and Tyr94^{L} that fix the conformation of heavy chain CDR loops for optimized hapten binding. Other somatic mutations including Ser30^{L}Asn, Glu42^{H}Lys, Gly65^{H}Asp, Asn76^{H}Lys, and Ala78^{H}Thr are also distant from the bound hapten, yet they reconfigure active site residues involved in binding interactions with hapten by reorganizing networks of hydrogen bonding, electrostatic and Van der Waals interactions between variable region residues over distances as long as 20 Å.

Thus, the structural studies on antibody 48G7 and its germline precursor again suggest that the germline antibody has an intrinsic structural flexibility and may undergo significant conformational changes to achieve better complementarity with the hapten. Somatic mutations serve to remove the CDR loop flexibility and preorganize the antibody combining site for hapten binding. These studies have also shown that somatic mutation can be either in the active site or significantly removed in distance, affecting ligand binding through coupled secondary sphere interactions such as sophisticated hydrogen bond networks. Similarly, mutational studies of enzymes have shown that one can significantly affect the binding and catalytic properties of enzymes through mutations outside the active site [47, 48], in much the same way as somatic mutations throughout the antibody variable region affect the antibody binding affinity. For an example, it was found in dihydrofolate reductase that two mutations, Arg44Leu and His45Gln, perturb the structure of the protein and elevate the pK_a of a folate binding site residue Asp27 (25 Å away from the site of the mutations) by one and two pH units, respectively [49]. In the case of β-lactamase, mutation Met182Thr, which is located 17 Å from the enzyme active site, is found to be responsible for the 500-fold increase in antibiotic resistance in combination with the two other mutations [50]. Structural studies suggest that the threonine hydroxy group introduced by this mutation forms two new hydrogen bonds with the backbone carbonyl groups of Glu63 and Glu64 and helps to fix the position of the catalytic residues [51]. The long-range effects of mutations in antibody and enzyme active sites suggest that distal regions of protein structures can be highly interconnected. This may be the structural basis for the evolution of allosteric binding sites in enzymes, in which changes at one binding site affect the binding of ligands at other sites that are spatially removed from each other.

The somatic mutations in antibody 48G7 have also been found to effect hapten binding in a context-dependent and cooperative manner. For example, analysis of the 48G7 crystal structure suggested that the somatic mutation Gly55^{H}Val may interact cooperatively with the somatic mutation Asn56^{H}Asp, since changes in the conformation of the turn in which residue 56^{H} resides appear to be induced by mutations at position 55^{H} (Fig. 1.12). The single reversion mutations Val55^{H}Gly and Asp56^{H}Asn were made in the affinity-matured antibody, as well as the double mutation in which both somatically introduced residues at 55^{H} and 56^{H} were switched back to their germline identities. Simple additive effects of the two single reversion mutations predicted a 0.4 kcal/mol loss in free energy of binding. However, the actual loss

of binding energy observed for 48G7 Val55^{H}Gly/Asp56^{H}Asn double mutant is 1.0 kcal/mol, with an additional 0.6 kcal/mol in binding free energy due to cooperativity between the sites of 55^{H} and 56^{H}. Cooperativity was also found between other proximal pairs of somatic mutations (30^{L}/34^{L} and 76^{H}/78^{H}), as well as between a non-proximal pair (55^{L}/76^{H}). Thus, the sources of a global gain in function may not always be delineated through changes in structure produced by individual mutations; cooperativity amongst somatic mutations may be another mechanism by which the immune system produces large increases in binding affinity for the affinity-matured antibody. This is well illustrated by the affinity maturation process of antibody 28B4.

1.6
Sulfur Oxidase Antibody 28B4 – Incremental Changes in Evolution

Antibody 28B4 catalyzes the periodate-dependent oxidation of sulfide **9** to sulfoxide **11** (Scheme 1.3) [25]. Hapten **12** was designed to mimic the transition state of the oxidation reaction using periodate as the cofactor. A total of nine replacement mutations, two in the light chain and seven in the heavy chain, occurred during the evolution of this antibody [25]. The X-ray crystal structures of the unliganded and hapten-bound germline Fab of antibody 28B4 were determined [26]. Comparison with the corresponding structures of the affinity-matured Fab of 28B4 [25] reveals the site of somatic mutations relative to the antibody combining site. Three of the mutations, Ser35^{H}Asn, Asn53^{H}Lys, and Asp95^{H}Trp, occur at the hapten-binding site; four mutations, Ser25^{L}Phe, Met34^{H}Phe, Val37^{H}Ala, and Ser76^{H}Gly, are one shell removed from the residues that form the hapten-binding pocket. The other two, Pro40^{L}Ser and Val12^{H}Gly, are close to the constant region of the antibody and far away from the bound hapten.

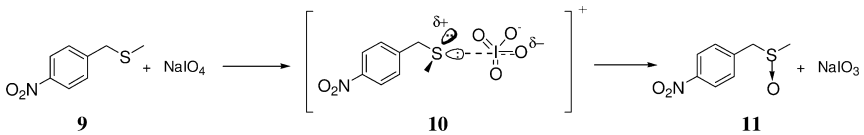

9 **10** **11**

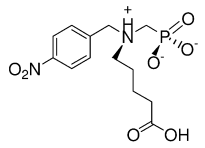

12

Scheme 1.3

Comparison of unbound and hapten **12**-bound germline Fab structures again shows that there are significant changes in the loops of CDR H3 and CDR L1 upon hapten binding. In the hapten-bound structure, residues H95 to H99 of CDR H3 are shifted away from hapten **12**. In the absence of such a CDR H3 conformational change, the backbone of $Tyr98^{H}$ would sterically clash with the *p*-nitro group of the bound hapten. The backward movement of the backbone of CDR H3 (a maximum of 3.7 Å between the Cα positions of $Tyr98^{H}$ in the two structures) removes this unfavorable steric interaction and at the same time introduces a new hydrogen bond between the backbone amide of $Ala99^{H}$ and the *p*-nitro oxygen atom of hapten **12**. $Asp95^{H}$ in this loop also makes hydrophobic contacts to the *p*-nitrophenyl ring of hapten **12**. There are also significant movements of residues L27c to L32 in the CDR L1 loop. Thus, a flexible, induced-fit type of binding mode is adopted by the germline antibody of 28B4 as with the other germline antibodies discussed so far. Comparison of the unliganded and hapten **12**-bound affinity-matured 28B4 structures shows that minimal changes occur upon hapten binding. This is again consistent with a lock-and-key mechanism of binding.

A comparison of the structures of the hapten-bound germline and affinity-matured Fab of antibody 28B4 reveals that hapten **12** is bound in different orientations in the two antibodies (Fig. 1.13). The somatic mutations at the antigen combining site of the germline antibody, $Ser35^{H}$Asn, $Asn53^{H}$Lys, and $Asp95^{H}$Trp, are mainly responsible for the new orientation adopted by the bound hapten in the affinity-matured antibody. While the phosphonate group of hapten **12** is bound in the same orientation in the two Fabs, the *p*-nitrophenyl ring of hapten **12** in 28B4 Fab is rotated relative to its orientation in the germline Fab and forms a parallel π-stacking interaction with the indole ring of $Trp95^{H}$ which was introduced by somatic mutation. The *p*-nitro group of the hapten is rotated away from $Glu34^{L}$ and forms a new hydrogen bond with the carboxamide group of somatically incorporated $Asn35^{H}$. The $Asn53^{H}$Lys somatic mutation introduces two new hydrogen bonds between the ε-amino group of $Lys53^{H}$ and the phosphonate moiety of hapten **12**. Thus, as a result of the active site mutations, hapten **12** has gained two additional hydrogen bonds to the phosphonate group and a higher degree of packing complementarity with residues $Trp95^{H}$, $Phe50^{H}$, $Tyr32^{L}$, and $Tyr36^{L}$. This is consistent with the 700-fold increase in hapten binding affinity of the affinity-matured antibody relative to the germline antibody.

An analysis of the binding affinities of pair-wise germline mutations reveals that their effects on hapten binding are coupled (Fig. 1.14). The single $Asp95^{H}$Trp mutation on the germline Fab results in a K_d of 450 nM, a 55-fold net gain in binding affinity relative to the germline Fab, whereas the K_d values of the $Ser35^{H}$Asn and $Asn53^{H}$Lys mutants are 31 μM and 27 μM, respectively, virtually unchanged from the germline Fab. This result suggests that the $Asp95^{H}$Trp mutation is largely responsible for switching the hapten from the germline to the affinity-matured binding orientation (Fig. 1.13). The π-stacking interactions involving $Trp95^{H}$ and $Tyr50^{H}$, which result from the $Asp95^{H}$Trp mutation, are clearly responsible for the altered binding geometry of the hapten in the affinity-matured antibody. In the germline Fab in which residue 95^{H} is Asp, the hapten is bound in a geometry far away from residues 35^{H} and 53^{H}, such that the somatically mutated residues $Asn35^{H}$ and $Lys53^{H}$ are too dis-

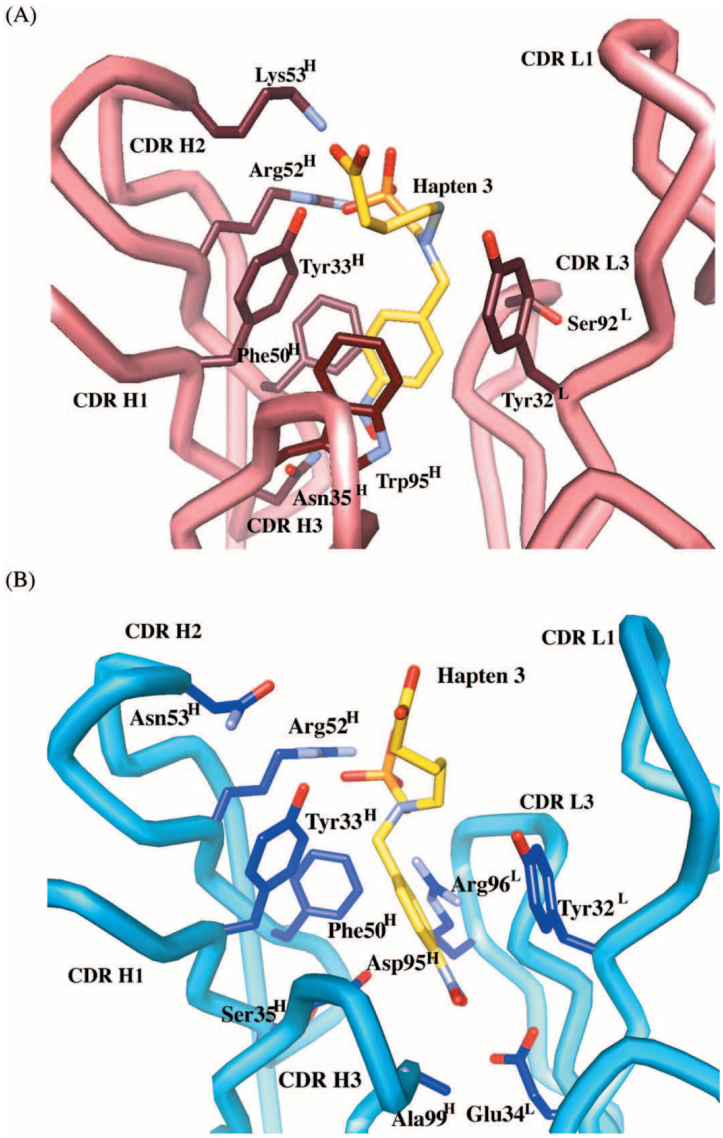

Fig. 1.13 Active sites of (**A**) the affinity-matured 28B4 Fab-hapten **12** complex (red) and (**B**) the germline Fab-hapten **12** complex (blue). Hapten **12** is in yellow.

tant to have any positive effect on hapten binding (Fig. 1.13). Thus, single somatic mutations at these sites alone do not increase the binding affinity of the germline antibody for the hapten. Indeed, the crystal structure of the germline antibody-hapten **12** complex shows that the closest distances between hapten **12** and $Ser35^{H}$ and $Asn53^{H}$ are 9.2 Å and 7.2 Å, respectively. However, the $Asp95^{H}Trp$ mutation leads

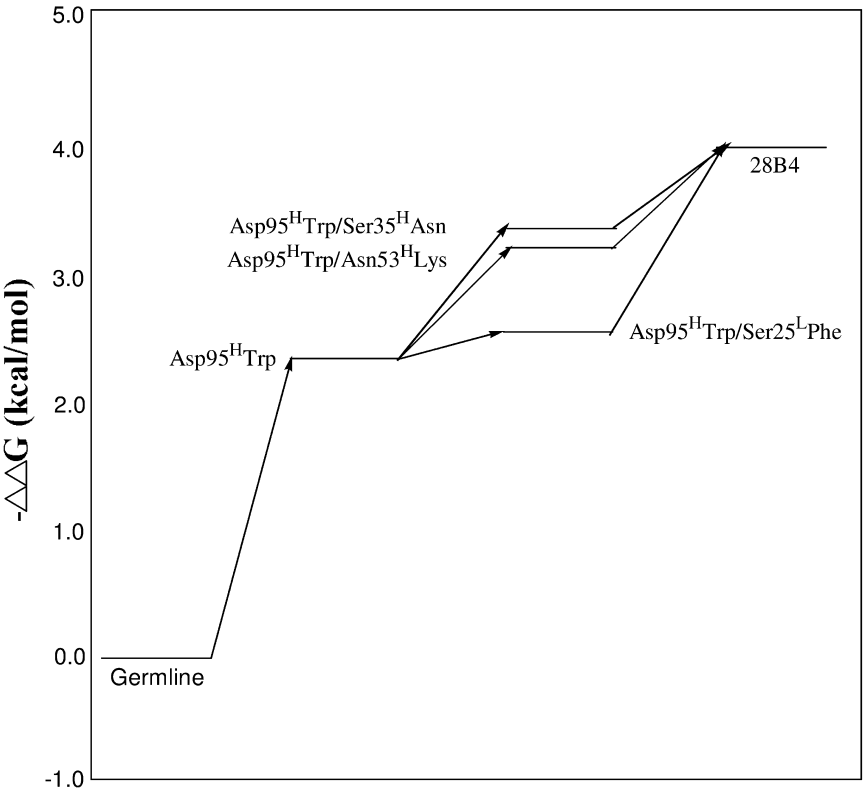

Fig. 1.14 Potential energy diagram showing that stepwise acquisition of somatic mutations by 28B4 germline antibody is accompanied by stepwise increase in binding affinity between the antibody and hapten **12**.

to a different orientation of the bound hapten, which allows $Asn35^{H}$ and $Lys53^{H}$ to make direct interactions with hapten **12**. The double mutants $Ser35^{H}Asn/Asp95^{H}Trp$ and $Asn53^{H}Lys/Asp95^{H}Trp$ have K_d values of 94 nM and 110 nM, respectively, corresponding to a roughly five-fold gain in binding affinity over the single somatic mutant $Asp95^{H}Trp$ (K_d = 450 nM).

These observations suggest that the somatic mutations $Ser35^{H}Asn$ and $Asn53^{H}Lys$ must have been introduced into an intermediate which had already acquired the $Asp95^{H}Trp$ mutation during previous rounds of mutation and selection. Thus, there is a stepwise acquisition of functional mutations by the germline antibody that concomitantly results in a stepwise increase in hapten-binding affinity (Fig. 1.14). This is most likely accomplished through an iterative cycle of mutation, affinity selection, and clonal expansion. A similar context-dependent effect has also been seen with the 48G7 antibody, [18] in which significant cooperativity was found between pairs of somatically mutated residues: together, the mutations have a much stronger favorable effect on hapten binding than a simple sum of the two individual effects.

One of Darwin's fundamental conclusions with regard to evolution is gradualism [52]. This theory appears to be applicable to the evolution of binding and catalysis in proteins as suggested by the evolution of catalytic antibody 28B4. Somatic mutations improve binding and/or catalytic function *incrementally* rather then in discontinuous jumps. In this way beneficial mutations from the previous round of selection are retained and incorporated in the next round of evolution. This realization is significantly changing the current mutagenesis strategies for the *in vitro* evolution of enzymes to better reflect those used by natural evolution [50].

1.7
Oxy-Cope Antibody AZ28 – Evolution of Conformational Diversity in Catalysis

The oxy-Cope reaction is a unimolecular [3,3] sigmatropic rearrangement that is widely used in organic synthesis but is not catalyzed by any known enzyme. Immunization with hapten **16**, a chair-like analog of the putative pericyclic transition state, led to the generation of catalytic antibody AZ-28 (Scheme 1.4) [12]. This antibody catalyzes the unimolecular oxy-Cope rearrangement of substrate **13** to product **15** with a rate acceleration (k_{cat}/k_{uncat}) of 5300, a K_m of 74 μM, and a K_d of 17 nM for hapten **16** [22]. During affinity maturation, the germline antibody acquired two somatic mutations in the light chain (Ser34^{L}Asn and Ala51^{L}Thr) and four in the heavy chain (Tyr32^{H}Phe, Ser56^{H}Gly, Asn58^{H}His, and Thr73^{H}Lys). As expected, the germline antibody has a lower binding affinity for hapten (K_d = 670 nM) than AZ-28, but surprisingly a higher catalytic rate: k_{cat}/k_{uncat} = 163 000 and K_m = 73 μM [22]. These values are close to that of chorismate mutase, which catalyzes the related [3, 3]-sigmatropic rearrangement of chorismate to prephenate [53].

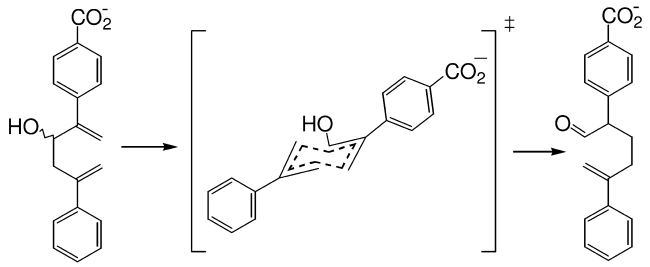

13 **14** **15**

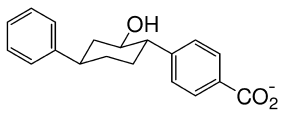

16

Scheme 1.4

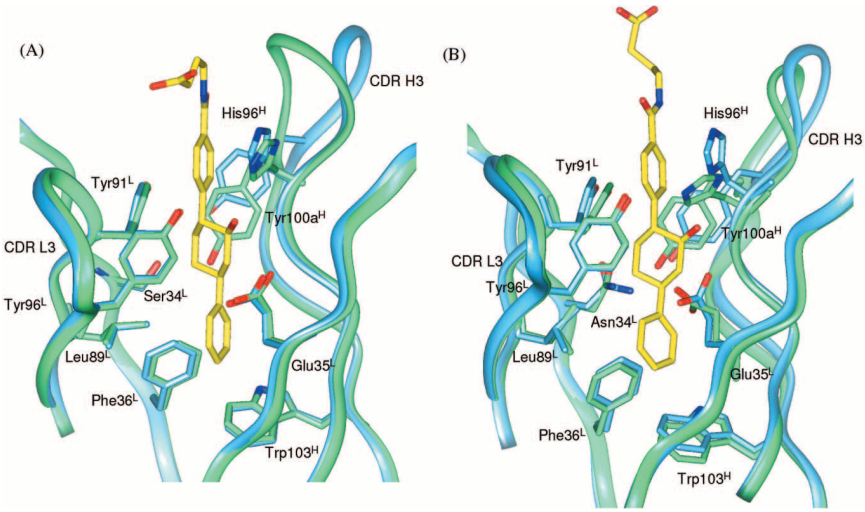

Fig. 1.15 (**A**) Overlay of the unliganded germline Fab (green) of antibody AZ28 and the germline Fab-hapten **16** complex (blue). (**B**) Overlay of the unliganded affinity-matured Fab (green) of antibody AZ28 and the affinity-matured Fab-hapten **16** complex (blue). Hapten **16** is in yellow.

To assess the structural basis for the decreased affinity but increased catalytic efficiency of the germline antibody, the X-ray crystal structures of the germline Fab and affinity-matured AZ28 Fab with and without hapten **16** bound were determined (Fig. 1.15) [23]. In the affinity-matured antibody, hapten **16** again binds in a lock-and-key mode with packing interactions between the antibody and 2,5-aryl substituents locking the substrate in the desired cyclic conformation. This is confirmed by NMR studies with TRNOE (transferred nuclear Overhauser effects) measurements showing that AZ28 preorganizes the normally extended substrate into a cyclic conformation so that its termini are in close proximity [54]. This leads to a cyclic alignment of the $4\pi + 2\sigma$ orbital system of the hexadiene core upon its binding to the antibody, lowering the overall entropy of activation ($\Delta S^{\neq}$) of the oxy-Cope reaction.

In addition, electronic effects arising from the 3-hydroxyl and 2,5-diphenyl substituents also affect the energetics of 3,3-sigmatropic rearrangement reactions. It is well known that anionic substituent effects accelerate the oxy-Cope rearrangement through hyperconjugation of electron density on oxygen [55]. Thus, $His96^H$ which hydrogen bonds to the 3-hydroxyl group of the substrate might act to enhance the rate of the rearrangement by increasing the electron density on the oxygen substituent of substrate **13**. Upon binding to the affinity-matured antibody, the cyclohexyl ring of hapten **16**, which mimics the cyclic $4\pi + 2\sigma$ transition state, is rotated out of the planes of the 5- and 2-phenyl rings by 81° and 83°, respectively. The two phenyl substituents are rotated with respect to each other by a dihedral angle of 19° and their conformations are fixed by the contacts with active-site residues, especially the π-stacking interactions between the 2-aryl substituent and $His96^H$, $Tyr91^L$, and $Tyr100a^H$. The aryl substituents at the 2 and 5 positions of the 1,5-hexadiene have been shown to lower

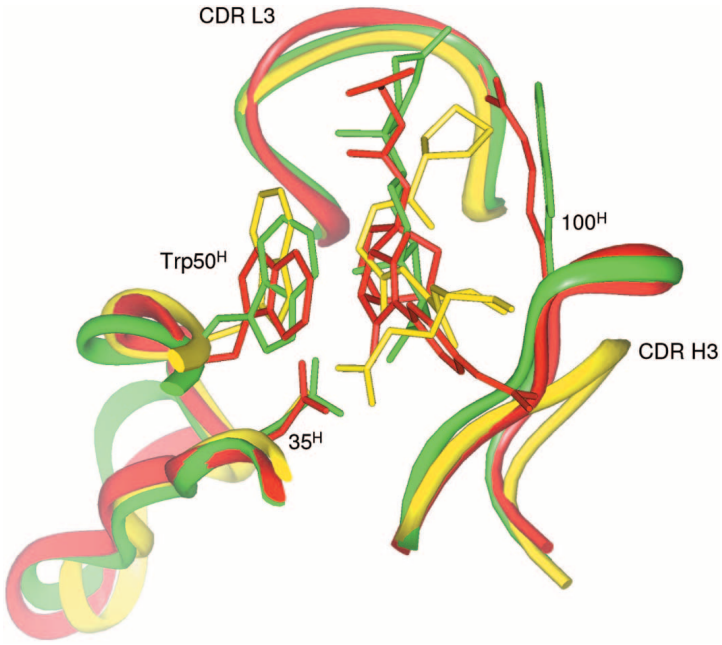

Fig. 1.16 Superposition of the CDR L3 and CDR H3 loops of antibodies DB3, TE33 and 39A11 with bound steroid (green), peptide (yellow) and hapten **20** (red), respectively.

the activation energy by 5–10 kcal/mol by stabilization of a biradicaloid-like transition state [56]. However, the crystal structure of AZ28 Fab-hapten **16** complex shows that the aryl substituents of hapten **16** are rotated out of planarity with the cyclohexyl ring, leading to decreased-orbital overlap. Thus it appears that the substrate is fixed in a catalytically unfavorable conformation upon its binding to the affinity-matured Fab.

The structures of the hapten-bound and free forms of the germline antibody provide an explanation for the increased rate of this antibody despite its lower affinity for hapten **16** (Fig. 1.15A). In the unliganded germline antibody structure, CDR H3 (residues $His96^H$ to $Asp101^H$) has a different conformation than that observed in the germline Fab-hapten **16** complex. Residue $Phe99^H$ (C_α) at the top of the loop is shifted 4.9 Å away from the hapten in the germline Fab-hapten complex relative to the unliganded structure. Such conformational flexibility in the germline antibody combining site would allow the 2-phenyl ring to rotate into planarity, increasing π overlap, and, as a result, lowering the activation energy.

The static snapshots of the oxy-Cope catalytic antibodies described here strongly suggest that the conformational diversity of the germline repertoire can also play a dynamic role in catalysis, much as (as is now being realized) side-chain dynamics play a key role in enzymatic catalysis. Indeed, a number of enzymes undergo conformational change upon binding of substrate and lead to enhanced catalytic rate, including hexokinase [42, 43] and triosephosphate isomerase [44]. Recent single-

molecule kinetic studies of enzyme-catalyzed reactions also suggest that different conformational states of proteins are characterized by different catalytic rates [57].

1.8
Diels-Alderase Antibody 39A11 – Evolution of a Polyspecific Antibody combining Site

Antibody 39A11 was generated to the bicyclo[2.2.2]octene hapten **20**, a mimic of the boat-like transition state of the Diels-Alder reaction (Scheme 1.5) [19]. This antibody catalyzes the cycloaddition reaction of diene **17** and dienophile **18** to give the Diels-Alder adduct **19**. The affinity maturation of antibody 39A11 results in only two somatic mutations: Val27c^{L}Leu in CDR L1 and Ser91^{L}Val in CDR L3 [20]. Mutagenesis studies suggest that somatic mutation Ser91^{L}Val is largely responsible for the 40-fold increase in binding affinity and 4-fold increase in k_{cat} for the affinity-matured Fab over the germline Fab. The X-ray crystal structures of the affinity-matured Fab with hapten **20** bound and the germline Fab unliganded were solved [20]. A comparison of the two structures indicates that neither somatic mutation nor ligand binding results in substantial structural or conformational changes in the active site. Thus the germline precursor to antibody 39A11 appears to be a good start point for the evolution of high-affinity combining site for hapten **20** – only one somatic mutation in the combining site is required to bind hapten with nano-molar affinity. It was further found that the germline antibody of 39A11 is polyspecific and shows binding for a panel of structurally very different ligands with affinity within an order of magnitude of that for its own hapten [20]. This polyspecificity may be general to several germline-encoded antibodies and may have been selected for by the immune system to provide

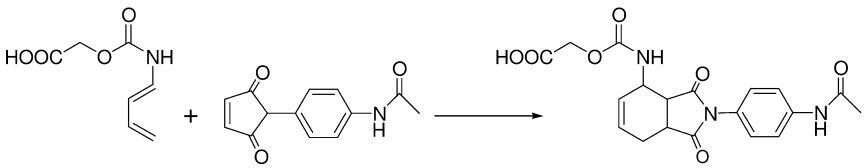

17 **18** **19**

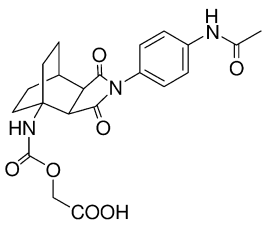

20

Scheme 1.5

a mechanism for rapid generation of antibodies of moderate to high affinity for a broad range of antigens.

Three other antibodies, DB3, TE33, and IE9 were raised against progesterone, a 16-amino acid peptide, and a hexachloronorbornene derivative [58–60], respectively, and are found to use V_H and V_L chains highly homologous to those of 39A11. Both DB3 and IE9 show some cross reactivity, and all four antibodies including 39A11 use a light chain variable region encoded by the Vκ1 gene, which is common to a relatively large population of antibodies that bind a large number of antigens including proteins, DNA, steroids, peptides, and small haptens [61]. However, all four antibodies have quite different CDR H3 loops. This suggests that certain combinations of Vκ–Jκ and V_H give rise to CDRs L1-3 and CDRs H1-2 that are responsible for the assembly of a partial antigen-combining site, which is polyspecific in nature. CDR H3, which is encoded by highly diverse D–J_H joining genes in each antibody, is responsible for the ultimate specificity of the fully assembled antibody. This notion is supported by a comparison of the X-ray crystal structures of DB3, TE33, and 39A11 (Fig. 1.15) [20, 58, 59]. Superposition of those structures reveals that the CDR H3 and CDR L3 loops, together with $Trp50^H$, form a deep hydrophobic binding pocket as the antibody combining site. In antibodies DB3 and 39A11, $Trp50^H$ and residue 100^H in the CDR H3 loop sandwich the hapten, providing critical hydrogen-bonding or hydrophobic contacts that define opposite walls of the deep binding pocket – $Trp100^H$ in DB3 packs with the central nonpolar region of the steroid, and $Arg100^H$ and $Trp50^H$ in 39A11 provide key hydrophobic and hydrogen-bonding interactions with hapten **20**. CDR H3 of antibody TE33 also packs on the C terminus of the peptide antigen. Thus, in these antibodies, CDR H3 is mainly responsible for the introduction of specific interactions into the antibody combining site that render the fully affinity-matured antibodies specific for their hapten. Such a strategy for variable region gene assembly would benefit the evolution of highly specific antibodies in two ways: (i) by increasing the diversity of the germline antibody binding repertoire, since a single combination of Vκ–Jκ and V_H can be used to construct combining sites for structurally very different antigens, and (ii) by accelerating the immunological evolution process, in that a single combination of Vκ–Jκ and V_H is polyspecific and can be tested in conjunction with all possible D–J_H joining genes for optimal antigen binding specificity and affinity. A similar strategy has also been used for the gene assembly of the germline antibody of 28B4 [26].

1.9 Conclusions

The immune system is able to generate high-affinity receptors for virtually any chemical structure through its ability to generate a large library of antibodies and to select members of the library based on the affinity of antibody with antigen. There are many parallels between this process and the natural evolution of enzymes. Consequently, studies of the immunological evolution of catalytic antibodies, as a prototypical exam-

ple of enzyme evolution, have provided a number of insights into the mechanisms of both antibody and enzyme evolution:

1. There is an intrinsic conformational flexibility within the germline antibody combining site. The binding of ligands to the germline antibody induces CDR loop conformational rearrangements that result in enhanced complementarity between the antibody and the ligand. The conformational diversity in the germline antibodies allows the immune system to evolve different antigen specificity using the same germline antibody scaffold, thus greatly expanding the germline binding repertoire. Such an "induced fit" binding mode in the germline antibody may have also existed in primitive proteins. Structural plasticity in the combining sites would have allowed a limited number of protein scaffolds to bind a broad array of substrates with moderate affinity. This plasticity might have allowed these proteins to catalyze a number of distinct reactions, albeit with low rate accelerations. Mutation and selection processes would optimize the complementarity of the protein active site with either a ligand (in the case of a simple receptor) or with a transition state (in the case of an enzyme), leading to enhanced catalytic efficiency and specificity. This process would provide an efficient way to allow a limited number of protein frameworks to evolve many distinct binding and catalytic functions.

2. Certain combinations of germline V genes (Vκ, Jκ and V_H) are polyspecific in nature and can be used to construct antibody combining sites for structurally very distinct ligands. CDR H3 (encoded by D_H–J_H joining) and later somatic mutations play a key role in defining the ultimate specificity of the antibody by introducing specific interactions that strengthen the binding of hapten or interfere with the binding of non-hapten ligands. Germline antibody polyspecificity further expands the binding potential of the germline repertoire.

3. Somatic mutations acquired by the affinity-matured antibody act to fix the conformation of the CDR loops and preorganize the antibody combining site to increase the complementarity with the hapten and/or introduce specific interactions that diminish the binding affinity for non-hapten ligands. This results in an antibody combining site with high specificity and affinity for the hapten in the affinity-matured antibody.

4. Somatic mutations can be introduced into the germline antibody at the peripheries of the hapten combining site that affect hapten binding through secondary sphere interactions, or they can occur at the hapten combining site and affect hapten binding by direct contact. Similarly, residues distal from the enzyme active site have been shown to have a long-range effect on enzyme catalysis.

5. The stepwise acquisition of functional mutations by the germline antibody genes is coupled with stepwise increases in binding affinity between antibody and antigen, often involving cooperative interactions.

This is manuscript 15490-CH of The Scripps Research Institute.

References

1 Pauling, L., *Chem. Eng. News* 24 (**1946**), p. 1375
2 Pauling, L., *Am. Scient.* 36 (**1948**), p. 51
3 Schultz, P. G., Yin, J., Lerner, R. A., *Angew. Chem. Int. Ed.* 41 (**2002**), p. 4427–4437
4 Gilbert, W., *Nature* 271 (**1978**), p. 501
5 Eigen, M., *Steps Towards Life, a Perspective on Evolution*, Oxford University Press, Oxford **1992**
6 Burnet, F. M., *The Clonal Selection Theory of Aquired Immunity*, Cambridge University Press, Cambridge **1959**
7 Talmage, D. W., *Science* 129 (**1959**), p. 1643
8 Tonegawa, S., *Nature* 302 (**1983**), p. 575–81
9 Janeway Jr, C. A., Travers, P., *Immunobiology, the Immunosystem in Health and Disease*, Current Biology Ltd., London **1997**
10 Jacobsen, J. R., Prudent, J. R., Kochersperger, L., Yonkovich, S., Schultz, P. G., *Science* 256 (**1992**), p. 365–7
11 Wirsching, P., Ashley, J. A., Benkovic, S. J., Janda, K. D., Lerner, R. A., *Science* 252 (**1991**), p. 680
12 Braisted, A. C., Schultz, P. G., *J. Am. Chem. Soc.* 116 (**1994**), p. 2211
13 Ma, L. F., Sweet, E. H., Schultz, P. G., *J. Am. Chem. Soc.* 121 (**1999**), p. 10227–10228
14 Ulrich, H. D., Patten, P. A., Yang, P. L., Romesberg, F. E., Schultz, P. G., *Proc. Natl. Acad. Sci. USA* 92 (**1995**), p. 11907–11
15 Patten, P. A., Gray, N. S., Yang, P. L., Marks, C. B., Wedemayer, G. J., Boniface, J. J., Stevens, R. C., Schultz, P. G., *Science* 271 (**1996**), p. 1086–91
16 Wedemayer, G. J., Wang, L. H., Patten, P. A., Schultz, P. G., Stevens, R. C., *J. Mol. Biol.* 268 (**1997**), p. 390–400
17 Wedemayer, G. J., Patten, P. A., Wang, L. H., Schultz, P. G., Stevens, R. C., *Science* 276 (**1997**), p. 1665–9
18 Yang, P. L., Schultz, P. G., *J. Mol. Biol.* 294 (**1999**), p. 1191–201
19 Braisted, A. C., Schultz, P. G., *J. Am. Chem. Soc.* 112 (**1990**), p. 7430
20 Romesberg, F. E., Spiller, B., Schultz, P. G., Stevens, R. C. *Science* 279 (**1998**), p. 1929–33
21 Romesberg, F. E., Schultz, P. G., *Bioorg. Med. Chem. Lett.* 9 (**1999**), p. 1741–4
22 Ulrich, H. D., Mundorff, E., Santarsiero, B. D., Driggers, E. M., Stevens, R. C., Schultz, P. G., *Nature* 389 (**1997**), p. 271–5
23 Mundorff, E. C., Hanson, M. A., Varvak, A., Ulrich, H., Schultz, P. G., and Stevens, R. C., *Biochemistry* 39 (**2000**), p. 627–32
24 Hsieh, L. C., Stephans, J. C., Schultz, P. G., *J. Am. Chem. Soc.* 116 (**1994**), p. 2167–2168

25 Hsieh-Wilson, L. C., Schultz, P. G., Stevens, R. C., *Proc. Natl. Acad. Sci. USA* 93 (**1996**), p. 5363–7

26 Yin, J., Mundorff, E. C., Yang, P. L., Wendt, K. U., Hanway, D., Stevens, R. C., Schultz, P. G., *Biochemistry* 40 (**2001**), p. 10764–73

27 Cochran, A. G., Schultz, P. G., *Science* 249 (**1990**), p. 781–3

28 Romesberg, F. E., Santarsiero, B. D., Spiller, B., Yin, J., Barnes, D., Schultz, P. G., Stevens, R. C., *Biochemistry* 37 (**1998**), p. 14404–9

29 Yin, J., Andryski, S., Beuscher, A. E., IV, Stevens, R. C., Schultz, P. G., (2003) *Proc. Natl. Aca. Sci.* (in press)

30 Yin, J., Beuscher, A. E., IV, Andryski, S., Stevens, R. C., Schultz, P. G., (2003) *J. Am. Chem. Soc.* (submitted)

31 Dailey, H. A., Dailey, T. A., Wu, C. K., Medlock, A. E., Wang, K. F., Rose, J. P., Wang, B. C., *Cell Mol. Life Sci.* 57 (**2000**), p. 1909–26

32 Dailey, H. A., Fleming, J. E., *J. Biol. Chem.* 258 (**1983**), p. 11453–9

33 McLaughlin, G. M., *J. Chem. Soc., Perkin Trans.* 2 (**1974**), p. 136

34 Blackwood, M. E., Jr., Rush, T. S., 3rd, Romesberg, F., Schultz, P. G., Spiro, T. G., *Biochemistry* 37 (**1998**), p. 779–82

35 Jentzen, W., Song, X. Z., Shelnutt, J. A., *J. Phys. Chem. B* 101 (**1997**), p. 1684–1699.

36 Haldane, J. B. S., *Enzymes*, Longmans Green, London **1930**, p. 182

37 Jencks, W. P., *Catalysis in Chemistry, and Enzymology*, McGraw-Hill, New York **1969**, p. 263

38 Fischer, E., *Ber.* 27 (**1894**), p. 3189

39 Koshland, D. E., Jr., *Proc. Natl. Acad. Sci. U. S. A.*, 44 (**1958**), p. 98–104

40 Wells, J. A., de Vos, A. M., *Annu. Rev. Biochem.* 65 (**1996**), p. 609–34

41 DeLano, W. L., Ultsch, M. H., de Vos, A. M., Wells, J. A., *Science* 287 (**2000**), p. 1279–83.

42 Anderson, W. F., Steitz, T. A., *J Mol Biol* 92 (**1975**), p. 279–87

43 DelaFuente, G., Lagunas, R., Sols, A., *Eur. J. Biochem.* 16 (**1970**), p. 226–33

44 Knowles, J. R., *Nature* 350 (**1991**), p. 121–4

45 Breinl, F., Haurowitz, F., *Z. Physiol. Chem.* 192 (**1930**), p. 45

46 Pauling, L., *J. Am. Chem. Soc.* 62 (**1940**), p. 2643

47 Baker, P. J., Waugh, M. L., Wang, X. G., Stillman, T. J., Turnbull, A. P., Engel, P. C., Rice, D. W., *Biochemistry* 36 (**1997**), p. 16109–15

48 Oue, S., Okamoto, A., Yano, T., Kagamiyama, H., *J. Biol. Chem.* 274 (**1999**), p. 2344–9

49 Adams, J., Johnson, K., Matthews, R., Benkovic, S. J. *Biochemistry* 28 (**1989**), p. 6611–6618

50 Stemmer, W. P., *Nature* 370 (**1994**), p. 389–91

51 Orencia, M. C., Yoon, J. S., Ness, J. E., Stemmer, W. P., Stevens, R. C., *Nat Struct Biol* 8 (**2001**), p. 238–42

52 Koshland, D. E., Jr. *Cold Spring Harb. Symp. Quant. Biol.* 52 (**1987**), p. 1–7

53 Andrews, P. R., Smith, G. D., Young, I. G., *Biochemistry* 12 (**1973**), p. 3492–8

54 Driggers, E. M., Cho, H. S., Liu, C. W., Katzka, C. P., Braisted, A. C., Ulrich, H. D., Wemmer, D. E., Schultz, P. G., *J. Am. Chem. Soc.* 120 (**1998**), p. 1945

55 Steigerwald, M. J., Goddard, W. A., Evans, D. A., *J. Am. Chem. Soc.* 101 (**1979**), p. 1994–1997

56 Dewar, M. J. S., Wade, L. E., *J. Am. Chem. Soc.* 99 (**1977**), p. 4417

57 Xie, X. S., Lu, H. P., *J. Biol. Chem.* 274 (**1999**), p. 15967–70

58 Arevalo, J. H., Taussig, M. J., Wilson, I. A., *Nature* 365 (**1993**), p. 859–63

59 Scherf, T., Hiller, R., Naider, F., Levitt, M., Anglister, J., *Biochemistry* 31 (**1992**), p. 6884–97

60 Haynes, M. et al., *Israel J. Chem.* 136 (**1996**), p. 151

61 Kim, H. et al., *J. Immunol.* 143 (**1989**), p. 638